Formation of Micelles in Homopolymer-Copolymer Mixtures: Quantitative Comparison between Simulations of Long Chains and Self-Consistent Field Calculations

A. Cavallo,[†] M. Müller,*[,‡] and K. Binder[†]

Institut für Physik, Johannes-Gutenberg-Universität, Staudinger-Weg 7, D-55099 Mainz, Germany, and Institut für Theoretische Physik, Georg-August-Universität, Friedrich-Hund-Platz 1, D-37077 Göttingen, Germany

Received July 4, 2006; Revised Manuscript Received September 15, 2006

ABSTRACT: Using Monte Carlo simulations of the bond fluctuation model and self-consistent field calculations, we study the formation of micelles in a mixture of homopolymers and asymmetric AB-diblock copolymers with composition, $f_A = 1/8$. Both types of molecules are fully flexible and have identical length. We work in the semi-grand-canonical ensemble, i.e., we fix the monomer density and incompatibility, $\chi N \simeq 100$ (strong segregation regime), and control the composition of the mixture via the exchange chemical potential, $\delta\mu \equiv \mu_{AB} - \mu_B$ between the copolymers and homopolymers. The Monte Carlo simulation comprises moves that allow homopolymers to mutate into AB-diblock copolymers and vice versa. These moves are very efficient in equilibrating the configurations. We accurately locate the critical micelle concentration, study the micellar size distribution and characterize the shape of the micelles by the tensor of gyration and radial density profiles. The results of the simulations are quantitatively compared to predictions of the self-consistent field theory in the grand-canonical ensemble without adjustable parameters. Only in the limit of high molecular weight the simulation results gradually approach the theoretical predictions.

I. Introduction

The formation of micelles is important for a variety of technological processes.[1−3] One application of copolymers consists of strengthening the interface between incompatible polymers. They segregate to the interface as to extend their blocks into the respective phases, thereby reducing the interface tension and increasing the number of entanglements across the interface.[4] Often the segregation of copolymers to the interface competes with the formation of micelles in the bulk. Thus, the concentration above which micelles form in the bulk, the critical micelle concentration (CMC), limits the amount of copolymers that one can use to compatibilize homopolymers and strengthen the interface.[5,6] More recently, block copolymer micelles have attracted much interest because their self-assembled structures in solution are significantly more stable than micelles formed by surfactants of low-molecular weight. The core of these "tough" micelles offers opportunities to utilize micelles for drug delivery.[7,8] The tunable and rather narrow size distribution of the micelle core can also be exploited to fabricate nanoparticles.[9]

For these reasons, the formation of micelles from amphiphilic molecules in solution has attracted abiding interest from experimentalists and theorists alike.[3,10] Micelles formed by diblock copolymers are of particular interest due to their applications and stability as well as due to their model character. Their size can be tuned by varying the molecular weight without changing the interactions, and the conformations of the macromolecules on large length scales are rather universal and well describable by simple chain models.

The free energy of a micelle results from an interplay between the free energy costs of the interface between the core and the corona/solvent and the entropy loss due to chain stretching.[11−17] Similar to the self-assembly of pure diblock copolymers, the interface tension favors large aggregates while the elastic energy limits the growth of their size. In the case of strong incompatibility, the corona forms a dense brush into which the solvent cannot penetrate, and the interface between corona and solvent gives rise to an additional tension (autophobicity).[18,19] If the micelle concentration is not very small, additional contributions due to the translational entropy of micelles and their interactions have to be accounted for.

The properties of micelles have extensively been studied by computer simulations.[20−36] Micelle formation is experimentally observed in amphiphilic systems that strongly differ in their chemical nature and in the mechanism which creates the repulsion between the two blocks that are joined together forming the amphiphile. Therefore, one expects that the universal properties of micelles can be described by coarse-grained models that only capture the relevant, amphiphilic nature of the molecule. Thus, it is tempting to use a model as simple as possible to investigate micelle formation. Potentially one can gain a lot in terms of computational convenience by replacing the interaction between the amphiphile and the solvent by an effective interaction between the amphiphilic beads. Those implicit solvent models have a long-standing tradition in polymer science and have attracted recent attention as efficient computer models to investigate membrane properties.[37−42] While there exists a formal one-to-one correspondence between the thermodynamic properties of an incompressible amphiphile−solvent mixture and the corresponding compressible, solvent-free amphiphile model with effective interactions, these effective interactions might not be well represented by density-independent pair potentials. For instance, by replacing the repulsion between solvent and polymer by an effective attraction between the polymer segments, one might observe a much higher local polymer density[43] than in the original, nearly incompressible mixture where the maximal value of the local polymer density is limited by the equation of state of the dense polymer melt.

[†] Institut für Physik, Johannes-Gutenberg-Universität.
[‡] Institut für Theoretische Physik, Georg-August-Universität.

10.1021/ma061493g CCC: $33.50
Published on Web 11/20/2006

Indeed, in solvent-free models of very short chains, micelles are readily observed. The simulations of model systems, however, fail to reproduce even qualitative predictions such as, e.g., the growth of the micelle with increasing chain length.[36] Since the assembly of diblock copolymers in solution is very similar to the micellization of low molecular weight surfactants in water or oil solution,[14−16] it is quite surprising that the analytical predictions break down completely for intermediate and small molecular weights.[36] The reasons for this discrepancy are unresolved. The quantitative comparison between simulations and predictions of scaling theories or self-consistent field calculations, however, faces difficulties: (i) The mapping between the computer model and the parameters of the analytical theory often remains unclear. The properties of micelles formed by short amphiphilic molecules depend on the details of the molecular architecture (e.g., stiffness of the molecule) and the local fluid structure (packing effects). Theory often considers the limit that the micelle size is large compared to the extension of a monomeric repeated unit. Only then the molecular characteristics can be described by a few coarse-grained parameters, e.g., the size of the amphiphilic blocks and their incompatibility, and the micelle comprises many amphiphilic molecules. (ii) Simulations in the canonical ensemble require extraordinarily large system sizes for the solution with a very low concentration of amphiphile to act as a reservoir. In a typical setting the concentration of the amphiphiles in solution significantly decreases upon formation of micelles. (iii) Simulations are severely hampered by difficulties to achieve thermal equilibrium. To sample the micelle size distribution in the canonical ensemble, amphiphiles have to be exchanged between micelle and reservoir or between different micelles. Since the solubility of the amphiphiles in solution is very low, this is a very slow process. One is tempted to use rather short chains to address this equilibration issue. In fact, most of the simulations use amphiphiles with less than 10 beads. In this case, however, the attraction between hydrophobic beads in a solvent-free model has to be very large to bring about the formation of micelles and the core of the micelle is very dense resulting in a sluggish dynamics and making the equilibration very difficult. We note that this is an artifact of solvent-free models. In the presence of solvent the micelle would form due to repulsion between solvent and hydrophobic segments rather than due to the strong attraction between hydrophobic entities. The total density of the mixture of solvent and amphiphile would not significantly increase in the core region and the mobility of the species would not dramatically slow as micelles form.

In the present work we quantitatively compare the results of large scale Monte Carlo simulations of long chains with predictions of numerical self-consistent field theory without adjustable parameters. Micellization has been studied by a variety of analytical techniques including scaling considerations[11−13] as well as the classical (strong-stretching) approximation.[16] These calculations allow for exploring the rich structures formed by copolymer-homopolymer mixtures as a function of incompatibility, molecular architecture and composition. The different analytical approaches and the regimes they predict have been compared in refs 15, 17, and 36. Because of the computational challenge posed by long chains, however, our simulations are restricted to a single value of chain composition and incompatibility. Rather than exploring the systematic dependence of the micelle size on system parameters, we focus on simultaneously comparing different micelle properties observed in the simulations to the quantitative predictions of the self-consistent field theory. Unlike other theoretical approaches, the self-consistent field theory invokes no other assumption than the applicability of the saddle point approximation.

We partially overcome the computational difficulties mentioned above by considering a mixture of an AB-diblock copolymer in a B-homopolymer-rich matrix that comprises chains of identical length. In our simulations we utilize the bond fluctuation model, a coarse-grained lattice model that often has served as a testing bed to compare simulations with self-consistent field theory.[44−46] We fix the degree of incompatibility $\chi N \simeq 100$ and consider very asymmetric diblocks with a ratio, $f_A = f = {}^1/_8$, between A and B monomers. For this architecture, the pure diblock will form spherical aggregates. Even if the corona was not swollen by the homopolymer solvent, its extension would be comparable to the radius of the core. In fact, homopolymers swell the corona, and the micelles are hairy and not crewcut. Thus, one expects micelles to adopt a spherical shape,[17] and we avoid possible complications due to the vicinity of the transition from a spherical to a cylindrical shape. The computational efficiency of the lattice model permits us to study rather long chains up to $N = 128$ effective segments and linear dimensions of the lattice up to $L = 96$. The structural symmetry of the copolymer and the homopolymer−solvent allows for an efficient simulation in the semi-grand-canonical ensemble, i.e., rather than fixing the number of copolymers in the simulation cell, we control the composition through the exchange potential, $\delta\mu$, between copolymers and solvent. Using an (almost) incompressible mixture of amphiphiles and solvent, the density in the micelle's core does not increase avoiding crystallization or vitrification.

Our manuscript is arranged as follows: In the next section we describe the simulation model and self-consistent field calculations. Then we discuss the thermodynamic and structural properties of the micelles. The manuscript concludes with a brief summary and outlook.

II. Model and Techniques

A. Monte Carlo Simulation. We consider a mixture of AB-diblock copolymers and B-homopolymers with the same degree of polymerization N. The diblock molecule has a very asymmetric composition − the fraction of (hydrophobic) A-monomers is $f = {}^1/_8$—leading to the formation of spherical aggregates already for the pure amphiphile.

We perform Monte Carlo simulations in the framework of the bond fluctuation model.[47−49] In this coarse-grained lattice model each monomer of a chain occupies eight lattice sites which constitute the vertices of a unit cube on a simple cubic lattice. Two consecutive monomers along a polymer are connected by fluctuating bonds, **b**. There are 108 possible bond vectors **b** yielding a good approximation of continuum space properties of flexible polymer chains. The volume fraction of occupied lattice sites is, $8\rho = 0.5$. At this density the model reproduces many features of a concentrated polymer solution or melt. Most notably the chain configurations are quite well described by Gaussian statistics down to rather small length scales. The linear extension of the simulation cell is $96u$ in units of the lattice spacing u and periodic boundary conditions are applied in all three spatial directions. Both the B-homopolymer solvent and the AB-diblock copolymers are comprised of the same number of effective segments, $N = 48$, 64, 96, and 128. For computational convenience, monomers interact via a square well potential that is extended over the nearest 54 lattice sites. These constitute the first neighbors shell in the monomer density pair correlation function.[49] Monomers of the same type attract each other while monomers of different species repel each other.

$\epsilon_{AB} = -\epsilon_{BB} = -\epsilon_{AA} \equiv \epsilon$. We keep the incompatibility per polymer fixed, $\epsilon N = 19.2$. The value of the incompatibility is chosen large enough for the corona and the core to be well segregated. Unlike the typical experimental situation, we do not fix the value of the incompatibility between segments, $\chi \sim \epsilon$, but between polymers $\chi N \sim \epsilon N$. Therefore, the width of the interface between core and corona, $w \sim a\sqrt{N}/\sqrt{\chi N}$, increases with chain length, N, and we do not expect the structure of the underlying lattice to be important for sufficiently large N. A relation between the interaction strength and the routinely utilized Flory−Huggins parameter is given by $\chi N \approx 2z_c\epsilon/k_BT$ where k_B is Boltzmann's constant and T denotes the temperature. In the following all energies are measured in units of the thermal energy scale, k_BT. For a homopolymer blend, the effective coordination number, z_c, can be identified with the number of monomers of other chains inside the interaction range.[44,49,50] This number slightly depends on the chain length due to the correlation hole effect and approaches the limit $N \rightarrow \infty$ with a $1/\sqrt{N}$-correction: $z_c = 2.1 + 2.8/\sqrt{N}$.[44] In the case of diblock copolymers it is unclear whether only interchain contacts or also interblock contacts contribute to micelle formation. Neglecting the chain length dependence of the effective coordination number, z_c, our choice of interaction strength corresponds to $\chi N \simeq 90$ ($\chi N \simeq 80$ for $z_c = 2.1$).

We work in the semi-grand-canonical ensemble[51] where the total number of chains in the system, $n_{AB} + n_B = n$, and the temperature, T, are fixed, but the composition of the mixture is allowed to fluctuate. The thermodynamically conjugated variable, the exchange chemical potential between copolymers and homopolymers, $\delta\mu \equiv \mu_{AB} - \mu_B$, is controlled. The semi-grand-canonical simulation scheme comprises two kinds of moves—semi-grand-canonical moves that switch the identity of homopolymers and copolymers but do not change their conformation and canonical moves that alter the chain conformations. We perform random local monomer displacements, where one moves a randomly chosen monomer by one lattice unit in a randomly chosen lattice direction, and slithering snakelike moves[44] where one removes a monomer at one randomly chosen end of the chain and attempts to attach it to the opposite end. All moves are subjected to the Metropolis acceptance criterion. The canonical moves relax the conformation of the chain on the lattice, the identity switches the composition of the mixture.

The choice of the semi-grand-canonical ensemble is crucial for the success of our simulations. (i) Due to the identity switches, the local composition relaxes much faster compared to simulations performed in the canonical ensemble where density fluctuations decay via the slow diffusion of insoluble copolymers through the B-homopolymer matrix, and it is also faster than simulations in the grand-canonical ensemble using the configurational bias algorithm and an implicit solvent model with strong attractions between core segments because the acceptance rate of semi-grand-canonical identity switches is much higher. (ii) In contrast to canonical simulations, the solvent properties (i.e., composition) do not depend on the micelle size. Simulations in the canonical ensemble would require intractably large system size to act as a reservoir. The speed up of the simulations makes possible the equilibration of very large micellar aggregates containing up to 10^4 monomers and to study their conformational properties, such as the radius of gyration of the micelles as a function of the chain length, density profiles, properties of interfaces, etc. While the use of the semi-grand-canonical ensemble for binary polymer blends[44,50−53] and homopolymer−copolymer mixtures[54,55] is standard, it has not yet been applied to study micellization.

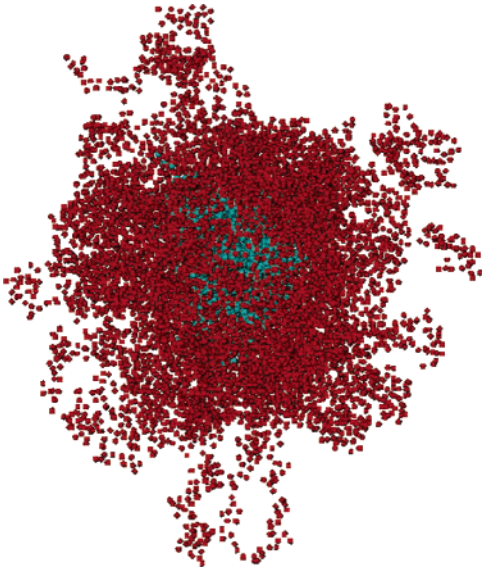

Figure 1. Snapshot of a micelle containing 77 copolymers with length $N = 128$ ($\approx 10^4$ monomers) at $\delta\mu = 6.0$. The solvophobic A segments are light gray (green) while the B segments of the corona are dark gray (red). The solvent is not shown.

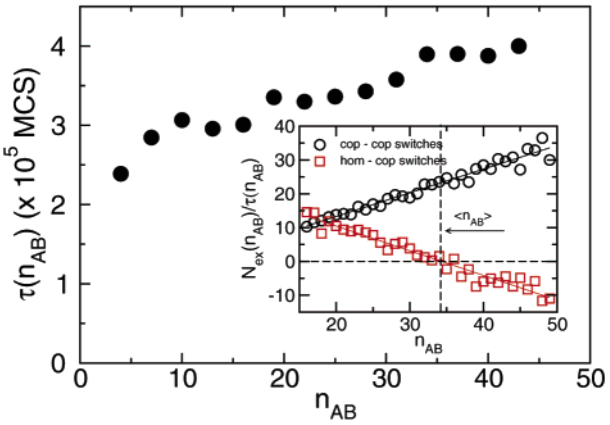

Figure 2. "Lifetime" $\tau(n_{AB})$ of the micelle, namely, number of MCS needed to renew completely the copolymers of a given micelle of size n_{AB} for $N = 48$ and $\delta\mu = 5.9$. In the inset the number of identity switches per unit "lifetime" $N_{ex}(n_{AB})/\tau(n_{AB})$ as a function of the cluster size n_{AB}. The vertical, dashed line marks the average micelle size $\langle n_{AB}\rangle$.

A snapshot of a micelle containing 77 copolymers with length $N = 128$ close to the cmc is shown in Figure 1. The efficiency of our algorithm has been quantitatively tested by analyzing the "lifetime" $\tau(n_{AB})$ of the clusters in the simulation box for different chain lengths as a function of the size n_{AB}. Because of the nonrealistic dynamics in the semi-grand-canonical ensemble, the meaning of "lifetime" is not the conventional one but it is defined as the number of Monte Carlo steps (MCS) needed to completely renew the elements of a micelle with a given size n_{AB}. This time has been estimated to be on the order of 10^5 MCS. To have a good statistics for the global properties of the micelles, all the averages have to be taken over much longer runs. An example of "lifetime" vs n_{AB} is given in Figure 2 for $N = 48$ and $\delta\mu = 5.9$. One can see that, even for the largest cluster, the relaxation time is on the order $\tau(n_{AB}) \approx 4.0 \times 10^5 \ll 10^8$. In the inset we analyze the number of identity switches $N_{ex}(n_{AB})/\tau(n_{AB})$ needed to renew completely the micelle. Note that exactly at $n_{AB} = \langle n_{AB}\rangle$, being $\langle n_{AB}\rangle$ the most probable micelle size, the number of homopolymer/copolymer switches in units of the "lifetime" equals the number of copolymer/homopolymer switches. Typically the simulation runs

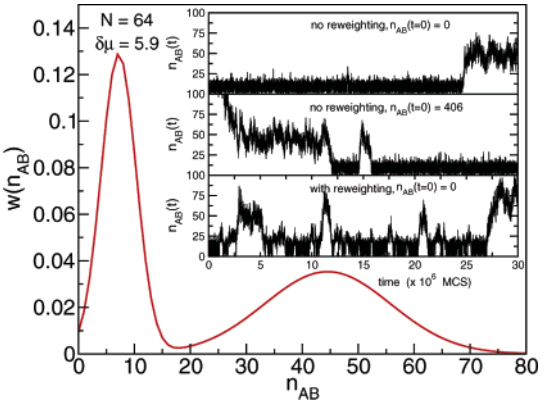

Figure 3. Probability distribution of the number of copolymers in the simulation box for $N = 64$ and $\delta\mu = 5.9$. This distribution has been utilized as weighting function w in the multicanonical simulations. Insets: Time development of the number of copolymers, n_{AB}, in the semi-grand-canonical simulations. The upper two panels show the evolution of nonreweighted runs using a homogeneous solution and a system that contains a micelle as starting configuration. The lower inset presents the time series for a reweighted simulation.

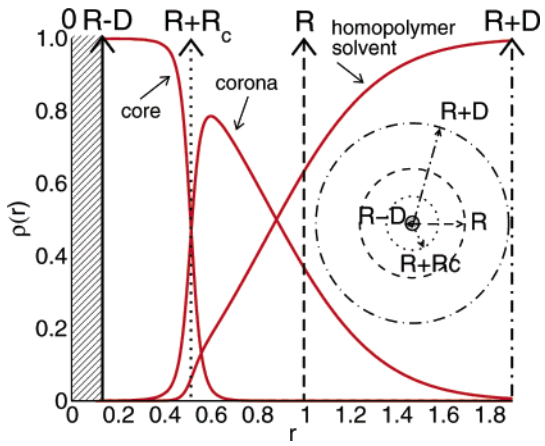

Figure 4. Typical density profile calculated using SCF theory and sketch of the system. In this plot we visualize the meaning of the parameters R, R_c, and D. Notice that our model, describing the spherical shell with internal radius $R - D$ and external radius $R + D$, does not give any prediction in the dashed region $0 \le r \le R - D$. The concomitant error committed can be minimized taking the limit $(R - D) \to 0$.

consist of $\mathcal{O}(10^8)$ MCS, exceeding by 2 or 3 orders of magnitude the "lifetime" of the clusters.

An important quantity that can readily be monitored in the course of the simulation is the micelle size distribution, $P(n_{AB})$. Below the cmc there are only small aggregates and their probability rapidly decreases with their size. In the vicinity of the cmc larger aggregates (i.e., micelles) form and the size distribution is bimodal—the two peaks correspond to a homogeneous solution (isolated copolymers or very small aggregates) and micelles, respectively. The two states are separated by a free energy barrier. Similar to a first-order phase transition this bimodal shape marks the cmc. Unlike the situation at a first-order transition, however, the barrier does not diverge in the thermodynamic limit, $L \to \infty$, because the micelle formation involves only a finite number of molecules (at finite chain length N) and there is no sharp transition in a thermodynamic sense. Nevertheless, micelles of long polymer chains comprise many molecules and the barrier may by far exceed the thermal energy scale, k_BT. To partially overcome the slowing down of the simulations due to the free energy barrier we apply for the largest chain length a multicanonical scheme.[53,56−60] To this end, we add to the original Hamiltonian of the system a preweighting function $k_BT \ln w(n_{AB})$ that only depends on the number of copolymers but not on their conformations. The choice $w(n_{AB}) \approx P(n_{AB})$ results in a uniform sampling of the size distribution. It removes the thermodynamic barrier, but of course, appropriate polymer conformations have to be generated in the course of transforming a homogeneous solution to a system that contains a micelle and vice versa. In Figure 3, we show the shape of the weight $w(n_{AB}) \approx P(n_{AB})$ we adopt in the reweighting scheme for a system of 864 polymers with length $N = 64$ at $\delta\mu = 5.9$. In the inset, we compare the "time evolution" of the number of copolymers in the system for different initial configurations. In the first two plots, no reweighting has been applied, in the last time series we adopt the above explained reweighting scheme which allows for a more frequent tunneling between the two states—homogeneous solution and micelle—containing on average 7 and 45 copolymers (see position of the two peaks in the distribution), respectively.

B. Self-Consistent Field Theory. In addition to Monte Carlo simulations we studied micelle formation within self-consistent field (SCF) theory[12,61−70] and provide quantitative predictions to which to compare the results of the Monte Carlo simulations. Our SCF technique in spherical geometry, similar to the work of Matsen,[71] has successfully been applied to study the elastic properties of interfaces in homopolymer−copolymer mixtures,[71,72] bubble nucleation,[73] and the micelle formation.[74] The latter work by Duque[74] is very similar to the present investigation except that we consider more asymmetric amphiphiles and a stronger incompatibility between unlike species.

We describe a mixture of AB-diblock copolymers and B-homopolymers in a spherical shell with radius R and thickness $2D$. The volume of the shell is $V = 4\pi[(R + D)^3 - (R - D)^3]/3$. To describe the entire micelles we extrapolate our SCF results to the limit $R \to D$. A typical profile calculated using SCFT together with a sketch of the system is presented in Figure 4.

The molecular composition, f, and the incompatibility per chain χN completely characterize the system within the SCF theory and, thus, SCF theory predicts all simulation data for different chain length N to collapse onto a single data set if lengths are measured in units of $R_e = a\sqrt{N}$.

Within the SCF theory one re-formulates the problem of interacting chains in terms of isolated chains in fluctuating fields, W_A, W_B, Ξ and Ψ. The grand-canonical free energy functional, $\mathcal{G}$, takes the following form:

$$\frac{N\mathcal{G}[\Phi_A, \Phi_B, W_A, W_B, \Xi, \Psi]}{k_BT\rho} = -z_h V \mathcal{Q}_h - z_c V \mathcal{Q}_c - \int d^3r\, [W_A(\mathbf{r})\Phi_A(\mathbf{r}) + W_B(\mathbf{r})\Phi_B(\mathbf{r})] + \int d^3r\, \chi N \Phi_A(\mathbf{r})\Phi_B(\mathbf{r}) + \int d^3r\, \Xi(\mathbf{r})[1 - \Phi_A(\mathbf{r}) - \Phi_B(\mathbf{r})] + -\Psi D \int d^3r\, \delta(|\mathbf{r}| - R_c)[\Phi_A(\mathbf{r}) - \Phi_B(\mathbf{r})]. \quad (1)$$

where z_h and z_c are the fugacities of B-homopolymers and AB-copolymers. Because of the incompressibility there is only one independent chemical potential and we set $z_h = 1$ and $z_c = \exp(\delta\mu/k_BT)$. $\mathcal{Q}_h$ and $\mathcal{Q}_c$ are the single-chain partition functions for the B-homopolymer and for the diblock copolymer in external fields, W_A and W_B that act on the A and B species, respectively. Ξ is a Lagrange multiplier that enforces incompressibility, $\phi_A(\mathbf{r}) + \phi_B(\mathbf{r}) = 1$, and Ψ is conjugated to the constraint

$$\phi_A(\mathbf{r}) = \phi_B(\mathbf{r}) \quad \text{on the shell } r = R_c \quad (2)$$

which dictates the size of the micelle. The latter allows us to

study the free energy of a micelle as a function of its size utilizing the constraint radius, R_c, as a reaction coordinate.

Within the mean field approximation the properties of a micelle are determined by the saddle point of the free energy functional $\mathcal{F}$. The stationary values of the fields are denoted by lower case letters. This yields the grand-canonical free energy $G(R_c) = \mathcal{F}[\phi_A, \phi_B, w_A, w_B, \xi, \psi]$ as a function of the micelle's radius R_c. This minimum of $G(R_c)$ with respect to R_c corresponds to the equilibrium micelle within mean field approximation and is characterized by $\psi(R_c) = 0$. The minimum of $G(R_c)$ coincides with the saddle point of the unconstraint functional (i.e., $\Psi \equiv 0$). Of course, the equilibrium is dictated by the unconstrained free energy minima. The constraint, however, allows us to calculate the free energy costs that correspond to increasing the number of amphiphiles in a micelle and to compare this quantity to the micelle size distribution observed in the simulations.

The excess grand-canonical free energy ΔG determines the stability of the micelle. It is obtained by comparing the free energy of a system that contains a micelle, G, with that of a homogeneous solvent, G_{hom}:

$$\Delta G = G - G_{hom} \tag{3}$$

The stationary fields are determined by the self-consistent set of equations:

$$w_A - w_B = -\chi N(\phi_A - \phi_B) - 2\psi D\delta(r - R_c) \tag{4}$$

$$\phi_A + \phi_B = 1 \tag{5}$$

$$\phi_A = z_c V \frac{\delta \mathcal{Q}_c}{\delta w_A} \tag{6}$$

$$\phi_B = z_h V \frac{\delta \mathcal{Q}_h}{\delta w_B} + z_c V \frac{\delta \mathcal{Q}_c}{\delta w_B} \tag{7}$$

$$\phi_A(R_c) = \phi_B(R_c) \tag{8}$$

The single chain partition functions, $\mathcal{Q}_h$ and $\mathcal{Q}_c$, can be expressed through the end-segment distribution functions, q_c, $q_c^\dagger$, and q_h via:

$$\mathcal{Q}_h = \int d^3\mathbf{r}\, q_h(\mathbf{r}, s) q_h(\mathbf{r}, 1 - s) \quad \forall s \tag{9}$$

$$\mathcal{Q}_c = \int d^3\mathbf{r}\, q_c(\mathbf{r}, s) q_c^\dagger(\mathbf{r}, 1 - s) \tag{10}$$

The end segment distribution functions, in turn, obey modified diffusion equations

$$\frac{\partial q_c(\mathbf{r}, s)}{\partial s} = \begin{Bmatrix} \left[\frac{Na^2}{6}\Delta - w_A(\mathbf{r})\right] q_c(\mathbf{r}, s), & 0 < s < f \\ \left[\frac{Na^2}{6}\Delta - w_B(\mathbf{r})\right] q_c(\mathbf{r}, s), & f < s < 1 \end{Bmatrix} \tag{11}$$

with initial condition $q_c(\mathbf{r}, 0) = 1$ and similarly for the propagator $q_c^\dagger$ that describes the copolymer conformations starting from the opposite end of the molecules. $R_e^2 = Na^2$ denotes the mean square end-to-end distance of the molecules. For the comparison with the Monte Carlo data we utilize the value $a = 3.4$ for all chain lengths. This value corresponds to the bulk statistical segment length in the limit $N \to \infty$. The segment distribution function of the B-homopolymer solvent obeys

$$\frac{\partial q_h(\mathbf{r}, s)}{\partial s} = \left[\frac{Na^2}{6}\Delta - w_B(\mathbf{r})\right] q_h(\mathbf{r}, s) \tag{12}$$

with $q_h(\mathbf{r}, 0) = 1$. These equations are solved by a spectral method. We consider only spherically symmetric micelles and expand spatially varying quantities, e.g., $\phi_A(r)$, in Fourier series $\phi_A(r) = \sum_{i=1}^{M} \phi_{Ai} f_i(r)$, where $\{f_i(r)\}_{i = 1,...,M}$ denote an orthonormal set of basis function.[66,71]

$$f_i(r) = \mathcal{N}_i \cos\left[\frac{(i-1)\pi(r - R - R_c + D)}{2D}\right] \tag{13}$$

with $\mathcal{N}_1 = 1$ and $\mathcal{N}_i = \sqrt{2}$ for $i = 2, ..., M$ and we choose $M = 118$. Thus, unlike the Monte Carlo simulations, fluctuations away from a perfectly spherical shape are not accounted for in the SCF calculations.

III. Critical Micelle Concentration (CMC)

The first step of our investigation is the measurement of the CMC, ϕ_{cmc}, or $\delta\mu_{cmc}$, as a function of the chain length, N, of copolymers. In our Monte Carlo simulations, we extract the cmc by monitoring the cluster size distribution $P(n_{AB})$ as a function of the chemical potential $\delta\mu$. In the vicinity of the CMC the distribution is bimodal and we define the location of the cmc as the chemical potential $\delta\mu_{cmc}$ at which the micellar and the homogeneous solution have equal weight. In the self-consistent field calculation the CMC can be identified by requiring that the excess grand-canonical free energy ΔG vanishes. Alternative definitions for the CMC can be envisioned that take into account the translational entropy of the micelles.[74]

As a first example, in Figure 5 we show the size distribution $P(n_{AB})$, obtained from Monte Carlo simulations, for $N = 48$ and increasing $\delta\mu$. In this case the bimodal shape of the distribution, which indicates the presence of micelles in the simulation box, builds up for $4.5 \le \delta\mu \le 5.8$. The bold line at $\delta\mu = 5.85$ indicates the distribution at the CMC. As we increase $\delta\mu$, the position of the Gaussian peak moves to larger aggregate sizes. In this plot we only report data up to $\delta\mu = 7.0$. For the largest values of $\delta\mu$, the tail of $P(n_{AB})$ signals the nonnegligible interaction between micelles. This asymmetric shape is the signature of the presence of big and elongated clusters formed by the overlapping of the cores of two neighboring spherical micelles. A proper analysis of these effects would require even larger system sizes, $L > 96$, which are beyond our computational resources.

The values of $\delta\mu_{cmc}$ and the corresponding ϕ_{cmc} vs $1/\sqrt{N}$ are shown in Figure 6 and compared to the SCF calculations for $\chi N \simeq 90$ and 100. From these data we can conclude that the chemical potential $\delta\mu_{cmc}$ apparently depends only slightly on the chain length. The agreement with the SCF result $\delta\mu = 5.78$ is rather good. In the inset we plot ϕ_{cmc} vs $1/\sqrt{N}$. In agreement with the corrections for $\delta\mu_{cmc}$, the concentration of copolymers needed to build a micelle also increases with chain length.

In our Monte Carlo simulations, we additionally monitor the adsorption isotherm, i.e., the average concentration of copolymers ϕ_{AB} in the system vs $\delta\mu$. Adsorption isotherms are easily accessible in experiments and they are often used to locate the CMC. The curves obtained by our Monte Carlo simulations for different degrees of polymerization are shown in Figure 7. The data points are presented on a semilogarithmic scale. In the limit of small copolymer concentration (low chemical potential) the density of copolymers increases linearly with $\delta\mu$. This behavior is in agreement with the Flory−Huggins expression of the

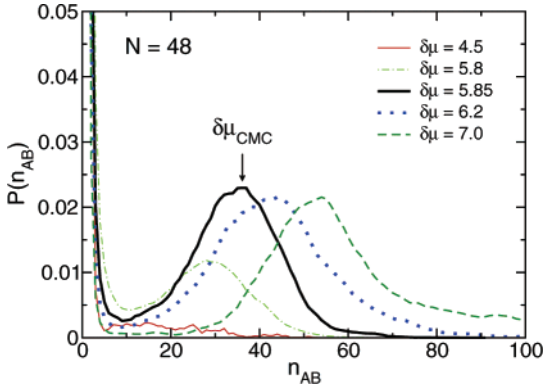

Figure 5. Cluster size distribution for chain length $N = 48$ and different values of $\delta\mu$. The bold curve denotes the size distribution at CMC. In this case the two peaks corresponding to the homogeneous solution and the micellar states are equally weighted. Note that, for $\delta\mu = 7.0$, the size distribution of micelles is no longer Gaussian. The tail in the distribution signals the presence of several micelles in the system and their interactions.

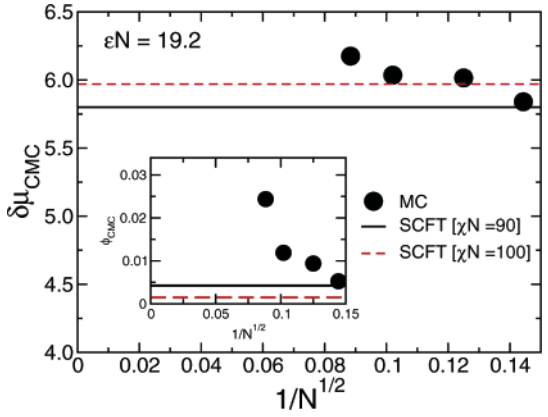

Figure 6. Chemical potential $\delta\mu_{cmc}$ as a function of $1/\sqrt{N}$. The inset shows the corresponding values of the critical micelle concentration ϕ_{cmc}. The full and dashed lines represent the SCF solutions, $\delta\mu_{cmc} = 5.78$, $\phi_{cmc} = 0.0042$ at $\chi N = 90$ and $\delta\mu_{cmc} = 5.97$, and $\phi_{cmc} = 0.00146$ at $\chi N = 100$.

chemical potential $\delta\mu$ written for small copolymer concentration, $\phi_{AB} \simeq 0$:

$$\delta\mu = \ln\frac{\phi_{AB}}{1-\phi_{AB}} - \chi N f\,(2f\phi_{AB} - 1) \approx \ln\phi_{AB} + \chi N f \quad (14)$$

A fit of the Monte Carlo data with eq 14 can provide an estimate of the degree of incompatibility χN for different chain lengths. The results are summarized in Table 1. The Flory−Huggins approximation, eq 14, only accounts for the translational entropy of the copolymers and the unfavorable interaction between the A-block and the B-solvent—the shrinking of the A-block in the bad solvent and the concomitant loss in conformational entropy is neglected.[49,75,76] This is a reasonable assumption for extremely large chain lengths and not too strong segregation. For the parameters of the simulations, however, the A-block shrinks as to increase the local A-density and enlarge the number of intra-block contacts reducing the number of contacts between unlike segments. Thus, the coordination number extracted from the adsorption isotherm will underestimate z_c and χN, respectively.

The full line in the plot gives the mean field eq 14 with $\chi N \simeq 90$. This value is obtained by extrapolating the results of the fit shown in Table 1 to the limit $N \to \infty$. The arrows on the ordinate mark the values of $\delta\mu_{cmc}$ at $\chi N \simeq 90$ and 100 obtained with SCF calculations.

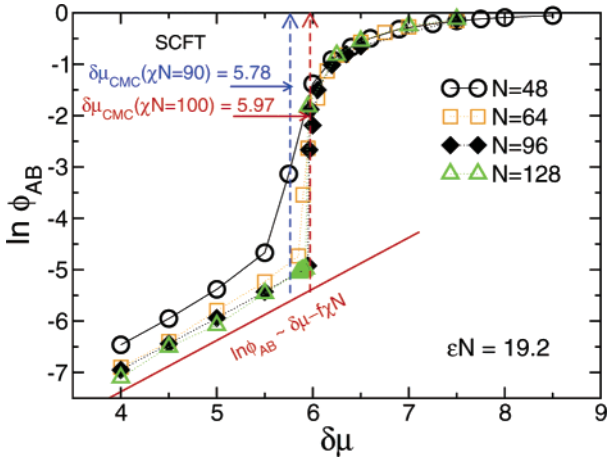

Figure 7. Fraction of copolymers ϕ_{AB} in the system plotted as a function of the chemical potential $\delta\mu$ for chain lengths $N = 48$, 64, 96, and 128 on a semilogarithmic scale. The full line indicates the mean field prediction given by eq 14 and the dashed lines the SCF theory predictions $\delta\mu_{cmc} = 5.78$ and $\delta\mu_{cmc} = 5.97$ at $\chi N = 90$ and 100, respectively.

Table 1. Fit of the Monte Carlo Data in the Case of Low Copolymer Concentration with the Equation $\ln\phi_{AB} = \delta\mu - f\chi N$ Utilizing χN as an Adjustable Parameter[a]

N	χN	$\tilde{z}_c$
48	82.92	2.16
64	86.26	2.25
96	87.36	2.27
128	87.72	2.28

[a] The corresponding coordination number, $\tilde{z}_c$, has been calculated using the relation $\tilde{z}_c \equiv \chi N/2\epsilon N$ (and not via the number of intermolecular contacts) with $\epsilon N = 19.2$.

In the interval $5.5 \le \delta\mu \le 6$, the adsorption isotherms exhibit an abrupt change in the concentration of copolymers in the simulation box. This provides clear evidence of the presence of large clusters in the system: the rearrangement of the coils involved in the formation of micelles and the reduced number of contacts between unlike species results in a rather rapid increase of the copolymer solubility of the mixture. Note that the longer the chain is the sharper ϕ_{AB} rises upward away from the logarithmic variation (see eq 14) before it approaches the asymptotic value $\phi_{AB} = 1$. Above the CMC, by comparing the total number of diblocks in the system and the number of diblocks forming clusters, we find that only a very small fraction of isolated copolymers, about 1%, is dispersed in the homopolymer−solvent. The majority fraction is involved in the formation of clusters or micelles. This picture is also true for larger values of $\delta\mu$. A quantitative analysis of the behavior of the cluster size, n_{AB}, vs N will be given in the next section.

For amphiphile concentration greatly exceeding the CMC other micelle shapes (wormlike micelles) have been detected in Monte Carlo simulations of very short chains[33] but we do not expect this complication arise for our asymmetric long amphiphiles. In the thermodynamic limit ($L \to \infty$), we rather expect the adsorption isotherm to develop a small jump at $\delta\mu > \delta\mu_{cmc}$ that signals the condensation of the fluid of micelles into an ordered lattice (with body centered cubic bcc structure). This first order transition between a disordered fluid and a bcc micellar phase, however, is not observed in our small simulation cells that contain only a few micelles.

IV. Micelle Size and Response to Fluctuations

In this section, we study the effect of the chain length N on the size distribution of micelles which are present in our Monte

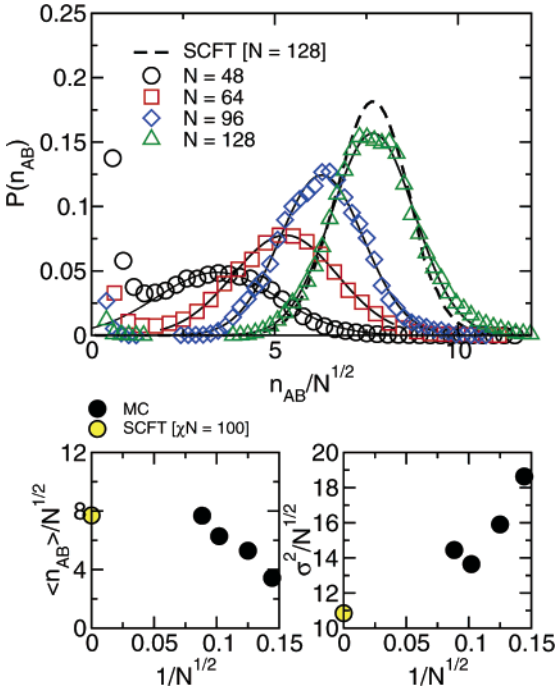

Figure 8. Upper panel: the cluster size distribution $P(n_{AB})$ as a function of the scaled aggregation number, $n_{AB}/\sqrt{N}$. The symbols represent the simulation data, the thick lines show the fit with a Gaussian function. For the largest chain length, $N = 128$, the SCF results for $\chi N = 100$ and $\delta\mu_{cmc} = 6.0$ are also shown as dashed line. The normalization of the SCF result was chosen such that the weight of the right peak (micelle) equals the result of the MC simulations. The MC data refer to concentrations slightly below the CMC. Lower panels: the behavior of the scaled average aggregation number, $\langle n_{AB}\rangle/\sqrt{N}$ and the scaled standard deviation $\sigma^2/\sqrt{N}$ as a function of $1/\sqrt{N}$. The latter data are obtained from the Gaussian fits of $P(n_{AB})$ in the upper panel.

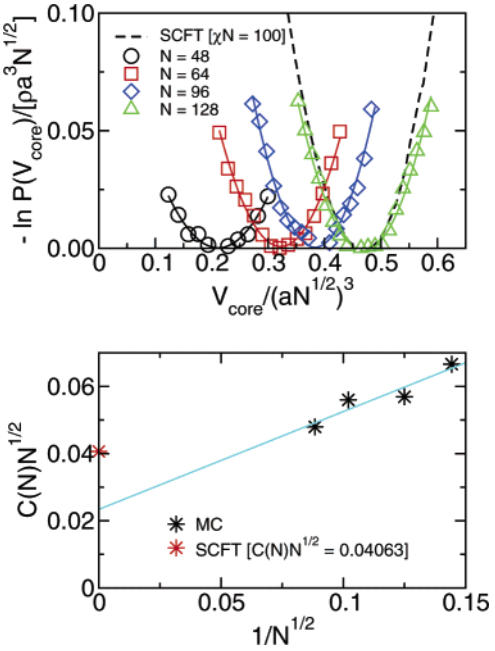

Figure 9. Upper panel: plot of the free energy $G(V_{core}) = -\ln P(V_{core})$ as a function of $\tilde{V}_{core} = V_{core}/(a\sqrt{N})^3 = 4\pi(R_{core}/a\sqrt{N})^3/3 = fn_{AB}/\rho a^3\sqrt{N}$. The lines represent fits of the free energy around the minimum with parabolic functions $G = a\tilde{V}^2_{core} + b\tilde{V}_{core} + c$. The curvature of the free energy at the minimum has been estimated by $C(N) = 1/2a$. Lower panel: curvatures for different chain lengths (dark stars) and the analogue result obtained by SCF theory (light star) vs $1/\sqrt{N}$.

Carlo simulations. In particular, we investigate the behavior of the average size of the clusters, $\langle n_{AB}\rangle$, vs N and the fluctuations around the most probable size. We can extract this information also from the SCF calculations by studying the minimum and the curvature of the excess free energy ΔG as a function of the volume of the core $V_{core} = 4\pi R_{core}{}^3/3$ (R_{core} being the radius of the core). Note that the scale of the grand-canonical free energy defined in eq 1 is set by $k_BT\rho a^3\sqrt{N}$. A direct comparison between the two methods is possible due to the relation $G(n_{AB}) = -k_BT \ln P(n_{AB})$, which connects the size distribution $P(n_{AB})$ to the free energy $G(n_{AB})$.

In Figure 8 (top), we present an enlarged view of the size distribution $P(n_{AB})$ around the peak corresponding to the micellar state for different chain lengths. The simulation data are obtained slightly below the CMC. Within the SCF theory the radius R_{core} of a micelle's core (at fixed χN) scales like the characteristic length, R_e. Therefore, $R_{core} \sim R_e \sim a\sqrt{N}$ and the number of chains per micelle is given by $n_{AB} = (\rho V_{core}/fN) = (4\pi\rho R_{core}{}^3/3fN) \sim \sqrt{N}$. Thus, we utilize $n_{AB}/\sqrt{N}$ as abscissa.

The top panel shows that the size of the micelles is Gaussianly distributed around the mean value $\langle n_{AB}\rangle$. The scaling plot reveals strong deviations: Instead of a data collapse we only observe a very gradual approach to the asymptotic behavior. The possible reasons for this behavior will be discussed in section 5. In any case, the growth of the micelle size with chain length is stronger than anticipated by the SCF theory.

In the bottom two panels of Figure 8, we show the results of the fit of $P(n_{AB})$ with a Gaussian distribution $g(n_{AB}) = (2\pi\sigma^2)^{-1/2}\exp[-(n_{AB} - \langle n_{AB}\rangle)^2/2\sigma^2]$ obtained for different N. On the left-hand side $\langle n_{AB}\rangle/N^{1/2}$ is plotted vs $1/\sqrt{N}$. This plot allows us to quantify the correction to the leading (mean field) behavior. Estimates of the fluctuations around the mean aggregation number, $\langle n_{AB}\rangle$ are given on the right-hand side where we display $\sigma^2/N^{1/2}$ vs $1/N^{1/2}$. This scaling is suggested by the SCF calculations: The free energy of a micelle scales like $G(n_{AB}) = k_BT\rho a^3\sqrt{N}\tilde{\mathcal{G}}(n_{AB}N/\rho(a\sqrt{N})^3)$ where $\tilde{\mathcal{G}}$ is a scaling function that depends on χN and $\delta\mu$. Thus, at a fixed incompatibility χN, the relative fluctuations of the micelle's size, $\sigma^2 \equiv \langle(n_{AB} - \langle n_{AB}\rangle)^2\rangle$ scale like $\rho a^3\sqrt{N}$.

The free energy, G, related to the size distribution in Figure 8 is shown in the upper panel of Figure 9. Here we have performed a variable transformation plotting G as a function of the volume of the micelle's core, $V_{core} = 4\pi R_{core}{}^3/3$. To investigate volume fluctuations we focus on the region around the minimum of the free energy. In the lower panel we plot an estimate of the curvature $C(N) \equiv \langle(V_{core} - \langle V_{core}{}^2\rangle)^2\rangle/(a\sqrt{N})^6$ times $\sqrt{N}$ (dark stars) vs $1/\sqrt{N}$. Note that this quantity is related to the fluctuations of the number of amphiphiles per micelle via $C(N) = (f/[\rho a^3\sqrt{N}])^2\langle(n_{AB} - \langle n_{AB}\rangle)^2\rangle \sim 1/[\rho a^3\sqrt{N}]$. The rescaled curvature extracted from the MC simulations extrapolates to a finite value which is compatible with the results of the SCF calculations (light star) for $N \to \infty$.

Figure 10 displays the excess free energy obtained by SCF theory for different values of χN at the CMC. Similar information has been obtained within the scaling considerations[15] and previous SCF calculations.[74] The data for $\chi N = 100$ are also plotted in the previous figure for comparison. As the incompatibility increases, the micelle size increases (cf. Figure 13) and the micelle size distribution becomes more narrow. The SCF calculations also allow to measure the free energy barrier associated with the formation of micelles assuming the micelle's radius as reaction coordinate. The barrier scales like $k_BT\rho R_{core}{}^3/N \sim \sqrt{N}$ upon increasing the chain length at fixed incompatibility, χN. This agrees with the observation that the free energy

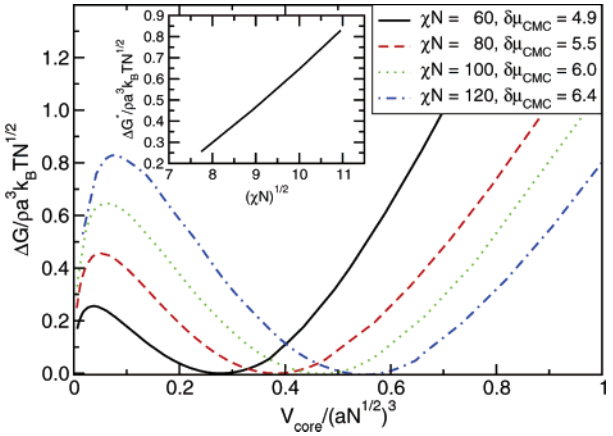

Figure 10. Excess free energy ΔG of the micelles (in units of $\rho a^3 \sqrt{N} k_B T$) calculated by SCF theory for different values of χN as a function of the normalized volume of the core $V_{core}/(a\sqrt{N})^3$. The curves are evaluated at fixed $\delta\mu_{cmc}$. The free energy landscape as a function of the reaction coordinate V_{core} exhibits a maximum that characterizes the barrier to form micelles and a minimum that corresponds to the stable micellar state. $\Delta G = 0$ at the minimum implies that the data are obtained at the CMC. In the inset, we plot the barrier ΔG^* vs $\sqrt{\chi N}$.

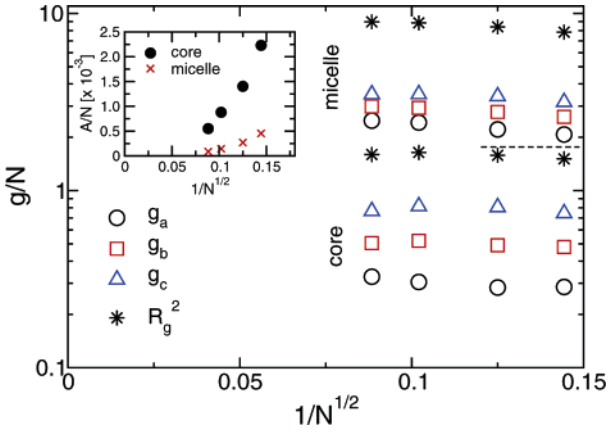

Figure 11. Eigenvalues, g_a, g_b and g_c, of the gyration tensor g divided by N as a function of $1/\sqrt{N}$. Both data for the whole micelle and the core are shown. In the same plot we also show the behavior of $R_g = g_a + g_b + g_b$. In the inset we plot asphericity, A, divided by N vs $1/\sqrt{N}$.

barrier between the homogeneous solution and micelles increases as we increase the chain length. This barrier height, ΔG^*, is important because it controls the equilibration times of micelles. In principle, the analogue information can also be extracted from MC results measuring the depth of the valley in Figure 8. The inset of Figure 10 shows the dependence of the barrier to micelle formation on the incompatibility. The barrier is related to the interface tension via $\Delta G^* \sim k_B T \rho a^3 \sqrt{N} \tilde{f}(\chi N) \sim \rho a^3 \sqrt{N} \gamma a^2 N \sim \rho a^3 \sqrt{N} \sqrt{\chi N}$ where $\tilde{f}$ is a scaling function that adopts the asymptotic behavior of the interface tension in the strong segregation limit. Indeed, when plotting ΔG^* vs $\sqrt{\chi N}$, we find a linear dependence over the range of incompatibilities investigated.

The shape and the dimension of the micelle can be characterized by the eigenvalues g_a, g_b, g_c ($g_a \le g_b \le g_c$) of the gyration tensor **g** with components:

$$g_{\alpha\beta} = \frac{1}{2N^2} \sum_{ij} [r_{i,\alpha} - r_{j,\alpha}][r_{i,\beta} - r_{j,\beta}] \qquad (15)$$

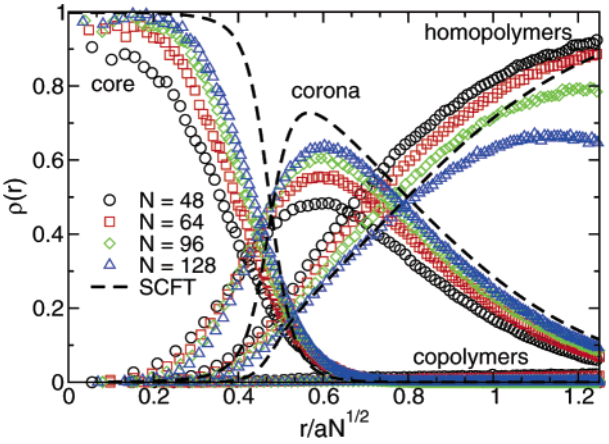

Figure 12. Radial density profile of core, corona, B-homopolymers, and isolated copolymers plotted as a function of $r/aN^{1/2}$ for different chain lengths. For $N = 48$ and $N = 64$, we choose configurations at chemical potentials $\delta\mu = 5.75$ and 5.95, for $N = 96$ and $N = 128$ we consider $\delta\mu$ slightly below $\delta\mu_{cmc}$. Finite-size effects occur at large r for $N = 96$ and $N = 128$. The dashed curves have been calculated using SCF theory for $\delta\mu = 5.78$ and $\chi N = 90$.

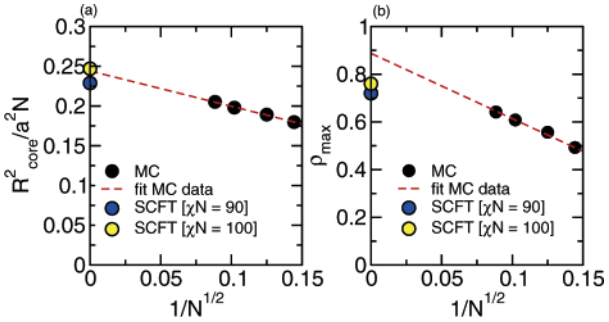

Figure 13. (a) R_{core}^2/a^2N, with R_{core} being the intersection point between the profiles of core and corona (core size) vs $1/N^{1/2}$. The red line, $y = 0.244 + 0.444x$, is the fit of the MC data. From this line we can extrapolate the value of $R_{core}^2/a^2N = 0.244$ in the limit $N \to \infty$ which is in good agreement with the prediction of the SCF theory for $\chi N = 100$ (open circle). (b) Height of the peak of the corona profile as a function of $1/N^{1/2}$. For $N \to \infty$ the MC simulations predict the value $\rho_{max} \approx 0.875$ which overestimates the SCF results for $\chi N = 90$ and 100.

where $r_{i,\alpha}$ is the $\alpha-$component of the position **r** of the ith monomer in a given chain ($i = 1,...,N$; $\alpha = x, y, z$). Note that

$$R_g^2 = g_a + g_b + g_c \qquad (16)$$

where R_g denotes the radius of gyration of the aggregate. A measure of the shape of the cluster is given by the asphericity A defined as

$$A = \frac{(g_a - g_b)^2 + (g_b - g_c)^2 + (g_c - g_a)^2}{2(g_a + g_b + g_c)^2}. \qquad (17)$$

A can assume values from 0 to 1. If $A = 0$ the micelle has a spherical symmetry. For $A = 1$, the micelle is a rod or a cylinder. The eigenvalues of the gyration tensor, the gyration radius and asphericity of the core and of the whole micelle, normalized by the chain length N, as a function of $1/\sqrt{N}$ are shown in Figure 11. The data for the three eigenvalues, g_a, g_b, g_c, and the gyration radius, R_g, show appreciable deviations from the ideal behavior only if they are calculated for the entire micelle. A fit of R_g vs N with the power law $R_g \sim N^\alpha$, yields the exponents $\alpha \approx 0.51$ and $\alpha \approx 0.56$ for the core and for the whole micelle, respectively. In the inset we plot the asphericity, A, of

the same systems vs $1/N^{1/2}$. These data strongly support a spherical shape for the micelles, $A \sim 10^{-3}$, for all chain lengths. The large error bars on this quantity do not allow us to make more quantitative statements about the shape fluctuations of the micelles as a function of chain length. The asphericity seems to decrease with N approaching the ideal value $A = 0$ for $N \rightarrow \infty$, and hence, one recovers the SCF result.

V. Radial Density Profiles and Interfaces

The radial density profiles around a micelle are presented in Figure 12. The profiles have been obtained by averaging over many micelles shifting the center of mass of each micelle to the origin of the coordinate system. All aggregates with size $\langle n_{AB} \rangle \pm 2\sigma$ contributed to the average. The figure shows the simulation data for chain lengths $N = 48$, 64, 96, and 128 by symbols whereas the predictions of the SCF theory for $\chi N = 90$ at the CMC ($\delta\mu_{cmc} = 5.78$) are displayed by lines. On the abscissa we plot the distance, r, from the micelle's center of mass in units of the molecules' end-to-end distance, $a\sqrt{N}$. For the two smaller N we used $\delta\mu = 5.75$ and 5.95, respectively, whereas, for $N = 96$ and $N = 128$, we fixed $\delta\mu = 6$. For the two larger chain lengths, the micelle size is unfortunately not much smaller than the linear extension, L of the simulation cell, and the homopolymer profile is somewhat distorted for large r.

In the profiles one can clearly distinguish a strongly segregated A-rich core that is separated by a sharp AB interface from the corona. The junction points of the amphiphiles are localized at this interface. For the incompatibility considered in the simulation the corona is swollen by the homopolymer solvent; i.e., the homopolymers penetrate the B-corona and reach up to the AB interface.

The plot confirms that the size of the micelle scales to leading order like $a\sqrt{N}$, but it also reveals corrections similar to those observed in Figure 8—rather than perfectly collapsing onto a single rescaled master curve, the simulation data gradually approach a limiting behavior which is compatible with the SCF predictions. The corrections to the asymptotic behavior can be traced back to three effects:

(i) The statistical segment length, $a \equiv (R_e/\sqrt{N\text{-}1})$, exhibits corrections to its leading, chain length independent asymptotic value. The A-blocks forming the core are rather short, $fN = 6$, 8, 12, 16, and on these small length scales, the excluded volume is not completely screened out; i.e., on length scales smaller than ξ_{ev} the chains are not ideal but they exhibit SAW statistics. For the bond fluctuation model at $8\rho = 0.5$, the screening length has been measured to be $\xi_{ev} \approx 7$;[78] this means that excluded volume effects are significant for chain sections of lengths $N_{ev} \approx \xi_{ev}^2/a^2 \approx 5$ where $a \approx 3.4$ denotes the segment length.

(ii) The Flory−Huggins parameter, χ, or the effective coordination number, z_c, exhibit strong $1/\sqrt{N}$-corrections to their leading, chain length independent asymptotic values due to correlation hole effects.

(iii) The size of the AB interface is broadened compared to the predictions of the SCF theory. These deviations stem from shape fluctuations of the micelle that are ignored within the mean field approximation.

To analyze more quantitatively to what extent the simulation data approach the SCF predictions for $N \rightarrow \infty$, we consider the chain length dependence of two characteristics of the profiles: (i) the radius R_{core} at which the A-density of the core equals the B-density of the corona yields an estimate of the micelle's size; (ii) the maximal density ρ_{max} of the B-segments of the amphiphiles in the corona yields information about the width of the AB interface and the penetration of the homopolymer solvent into the corona. In Figure 13, we plot those two quantities, R_{core} and ρ_{max}, vs $1/\sqrt{N}$ in order to extrapolate them by a linear fit to the limit $N \rightarrow \infty$ and quantitatively compare the asymptotic values with the SCF calculations at the CMC for $\chi N = 90$ and 100. The chain length dependence of the simulation results is well described by a $1/\sqrt{N}$-correction. The asymptotic value of the core radius, R_{core}, quantitatively agrees with the predictions of the SCF theory while we find that the asymptotic value of the maximal B-density of the corona is about 20% larger than the SCF calculations. The latter discrepancy might partially be attributed to the effects of the small simulation cell that might affect the details of the profiles more significantly than the micelle's radius.

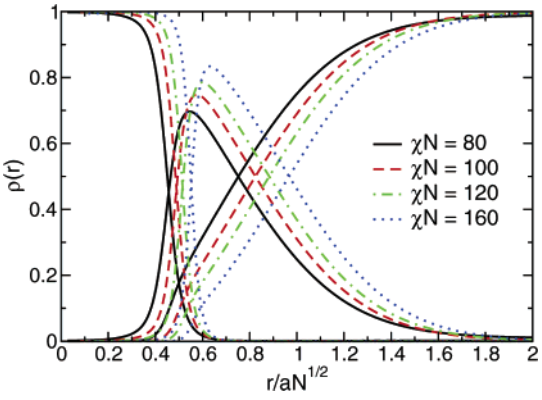

Figure 14. Radial density profiles as obtained from SCF calculations for different values of χN at CMC. The increase of the incompatibility between A- and B-blocks causes the sharpening of the interface core−corona and the progressive expulsion of the homopolymer/solvent from the corona shell.

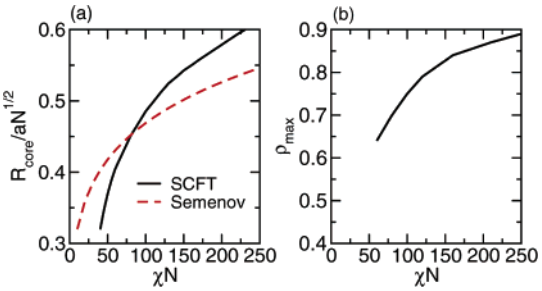

Figure 15. (a) Plot of the normalized core radius obtained by SCF calculations as a function of χN. These results are compared to the theoretical prediction, $R_{core}/aN^{1/2} = 2.18(f/6)^{1/2}(f\chi N)^{1/6}$, by Semenov[77] in the strong segregation limit. (b) Height of the peak of the corona profile vs χN.

To explore the role of incompatibility, we present in Figure 14 the dependence of the profiles in the interval $80 \leq \chi N \leq 160$. This illustrates the effects associated with the uncertainty of the identification of the Flory−Huggins parameter, χ, and it is also interesting in its own right. As we increase χN the radius of the core increases (cf. panel a), the distribution of the junction points between the two blocks becomes sharper, and the maximal density in the corona increases. In Figure 15 we plot the rescaled core size, $R_{core}/(a\sqrt{N})$, and the peak of the corona profile ρ_{max} as a function of χN. Panel a compares our SCF calculations for $R_{core}/aN^{1/2}$ to Semenov's result[77] $R_{core}/(a\sqrt{N}) = 2.18(f/6)^{1/2}(f\chi N)^{1/6}$ for block copolymer micelles in the strong segregation limit assuming that the homopolymer solvent penetrates the corona (wet brush). The analytical prediction overestimates the micelle size for low and intermediate segregation, $40 \lesssim \chi N \lesssim 80$. This is quite expected because, e.g., the strong segregation approximation overestimates the AB interface tension.[79] Other corrections to the strong segregation ap-

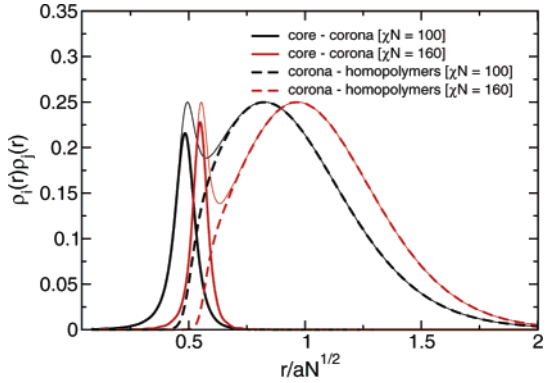

Figure 16. Interfaces core−corona (solid line) and corona-homopolymers (dashed lines) for $\chi N = 100$ and 160. For the degrees of incompatibility we have examined the two interfaces always overlap, this means that we find a nonnegligible concentration of homopolymer/solvent in the shell around the core where the junction between the two blocks are located. The thin curves represent the sum of the two overlapping interfaces. For very high values of χN we expect that the two interfaces will be independent.

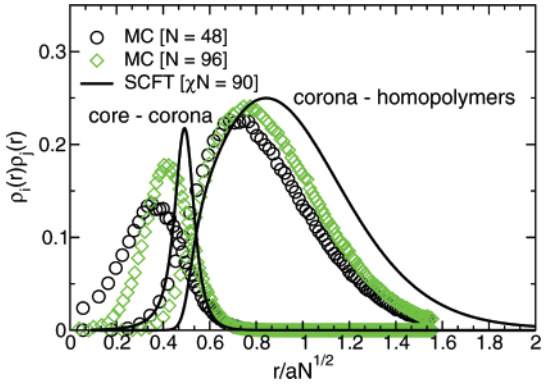

Figure 17. Plot of the interfaces core−corona and corona-homopolymers for $N = 48$ and 96. The MC data are compared to the SCF calculations for $\chi N = 90$.

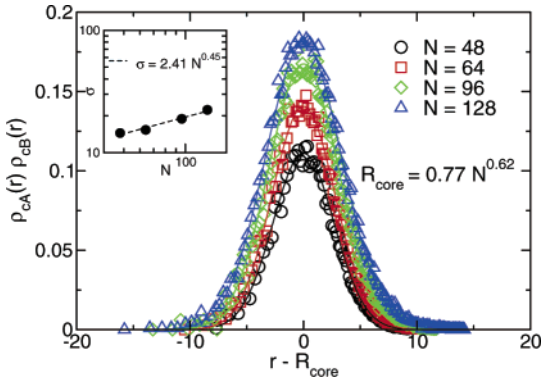

Figure 18. Product of the radial density profiles of core and corona, $\rho_{cA}(r)\rho_{cB}(r)$, plotted as a function of $r - R_{core}$ with R_{core} being the average position of the junctions or intersection point of the core and corona profiles. The curves can be fitted with a Gaussian function peaked at R_{core} and with standard deviation σ. The fit gives $R_{core} = 0.77N^{0.62}$ and $\sigma = 2.41N^{0.45}$. The latter power-law and the corresponding data points are shown in the inset.

proximation have been discussed by Likhtman and Semenov.[80] Since the micelle's size results from a balance between the cost of the AB interface per chain which tends to increase its radius and the stretching required to fill space uniformly which tends to decrease R_{core}, a smaller interface tension gives rise to a smaller micelle size. At large incompatibilities, however, the strong stretching theory underestimates the micelle size. This might be due to the fact that at large χN the corona becomes so dense that the homopolymers cannot penetrate it. In this limit, the dense corona resembles a dry brush and an interface between corona and melt gradually builds up (autophobicity[18,19]) as we increase χN. Asymptotically, there are three layers—core, corona, and B-homopolymers—that consist of pure A-segments, of only B-segments of the amphiphiles, and of solvent segments, respectively. These three layers are separated by narrow interfaces. The free energy cost that is associated with the second corona−melt interface tends to additionally increase the micelle size.

The building up of two distinct interfaces, their position and width can be monitored by the product of the corresponding densities, $\rho_{cA}(r)\rho_{cB}(r)$ for the core−corona interface and $\rho_{cB}(r)\rho_{hB}(r)$ for the corona−melt interface, respectively.

The predictions of the SCF theory are presented in Figure 16. One observes that the core−corona and corona−melt interfaces become more separated, the maximal density of B-corona segments increases, and the corona−melt interface moves further outward as we increase the incompatibility. When measured in units of the natural size $R_e = a\sqrt{N}$, the AB-interface sharpens but the width of the corona−melt interface does not significantly change upon increasing χN from 100 to 160.

Figure 17 shows the simulation data for $N = 48$ and 96—the shortest chain length is not affected by the limitation of the simulation cell—and compares them to the predictions of the SCF theory for $\chi N = 90$. The AB interface is much sharper in the SCF calculations than in the simulations signaling the rather pronounced shape fluctuations of small micelles. As the chain length increases, however, the interface becomes narrower and moves further outward, thereby improving the agreement with the SCF calculations. For the incompatibility used in the simulations, the homopolymers penetrate the corona and the product of the corona and melt densities has a very broad peak which also moves slightly outward with increasing chain length but does not significantly sharpen.

In Figure 18, we display the product $\rho_{cA}(r)\rho_{cB}(r)$ assuming that the inner arrangement of the micelle is not strongly affected by the size of the simulation cell. From the graph, we extract the chain length dependence of the width of the AB interface defined as the variance of the peak when fitted by a Gaussian distribution. The chain length dependence is describable by an apparent power law of the form $\sigma = 2.14N^{0.45}$ and a similar fit also yields $R_{core} = 0.77N^{0.62}$. Both apparent exponents are close to the square-root dependence of the SCF calculations. The narrow overlap core−corona can be fitted by a Gaussian function, on the contrary, the broader overlap corona-homopolymers exhibit a non symmetric decay. From these curves we also obtain an estimate of the number of copolymers per unit surface defined as $\langle n_{AB}\rangle/4\pi R_{core}^2 \sim N^{-1/2}$ as a function of chain length close to the CMC. The corresponding data are plotted in Figure 19. This quantity can also be seen as the "grafting density" of a brush (corona shell) on a spherical surface (core).

VI. Conformational Properties of A- and B-Blocks Inside the Micelle

One reason for the deviations between the MC simulations and the SCF calculations for finite chain length are deviations from the Gaussian chain behavior. These are particularly important because (i) the chain conformations in a micelle differ from their bulk behavior and (ii) the amphiphilic architecture is not well describable by the Gaussian chain model on short

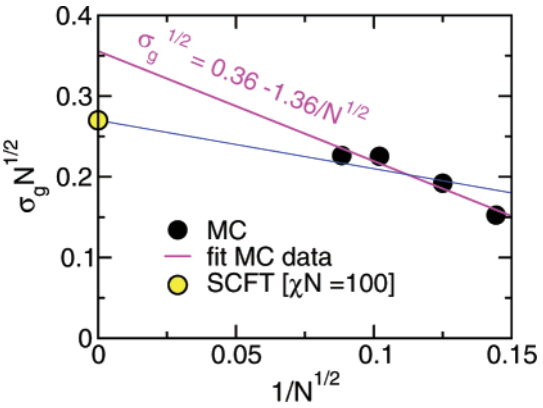

Figure 19. Number of copolymers per unit surface $\sigma_g = n_{AB}/4\pi R_{core}^2$ times $N^{1/2}$ as a function of $1/N^{1/2}$. The MC data are compared to the analogous SCF theory result at $\chi N = 100$. A linear fit of the simulation data gives the expression $\sigma_g N^{1/2} = 0.36 - 1.36/N^{1/2}$ overestimating the SCF theory prediction, $\sigma_g N^{1/2} = 0.27$, in the limit $N \to \infty$. An alternative straight line forced to start at the SCF calculations is also included.

Table 2. Conformational Properties of Amphiphiles in a Micelle

N	$\delta\mu$	$R_{e,A}$	$R_{e,B}$	R_{core}	σ_g
48	5.75	5.76	20.20	9.41	0.176
48	5.80	5.78	20.30	9.66	0.184
48	6.00	5.86	20.28	10.42	0.208
48	6.10	5.87	20.30	10.74	0.212
48	6.20	5.91	20.21	11.02	0.216
48	6.40	5.975	20.26	11.99	0.232
48	6.50	5.97	20.14	11.93	0.232
48	8.50	5.99	19.66	12.16	0.248
64	5.95[a]	7.16	24.17	11.69	0.192
96	6.00[a]	9.39	30.41	14.69	0.184
128	6.00[a]	11.26	36.62	16.84	0.160

[a] $\delta\mu \lesssim \delta\mu_{cmc}$.

length scales (e.g., swelling of the conformations ($< \xi_{ev}$) due to unscreened excluded volume interactions). The pertinent MC data are summarized in Table 2.

In Figure 20a, we quantify the average degree of stretching by presenting the mean squared end-to-end distance, R_e^2, of the A- and B-blocks normalized by the number of segments, N_{bl}, of a block. The simulation data for A-blocks and B-blocks are well described by $R_{eA}^2 = 11.70N_{bl} - 15.05N_{bl}^{1/2}$ and $R_{eB}^2 = 15.13N_{bl} - 35.37N_{bl}^{1/2}$, respectively. The outer B-blocks are stretched, $R_{eB}^2/a^2N_{bl} \to 1.48$. In panel (b) we plot $R_e^2(s)/s$ vs the curvilinear distance, s, from the junction point. $R_e(s)$ denotes the end-to-end distance between the s^{th} monomer in the corona and the junction point. For large s we observe a plateau indicating the rather uniform Gaussian stretching along the B-block. The deviations at small s stem from the nontrivial local structure (local stiffness and excluded volume). These effects are not captured by the SCF theory but enter the description only via the statistical segment length, a. The data for the A-core are shown in the inset. Since they are comprised of fewer segments the deviations from the Gaussian behavior influence a larger fraction and only for the largest chain length $N = 128$ a plateau gradually develops. We also note that the bond that joins the two blocks is strongly stretched because the range of the repulsion between unlike species is smaller than the maximal bond length.

Upon increasing the chemical potential, we observe that the aggregation number and also the effective grafting density σ_g of the blocks at the AB-interface increase (cf. data for $N = 48$ in Table 2). The A-blocks stretch further due to the larger R_{core} but the corona is only slightly perturbed.

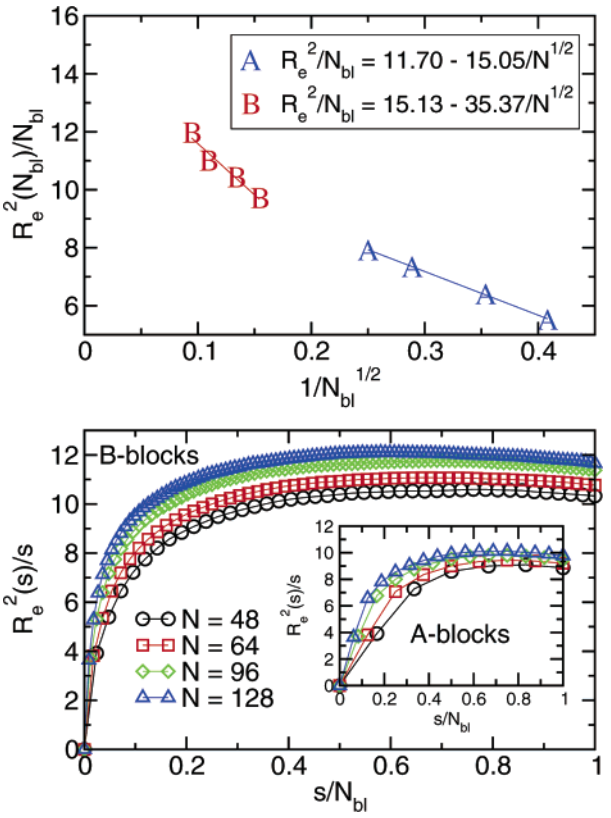

Figure 20. (a) Normalized mean squared end-to-end distance, R_e^2/N_{bl}, of A- and B-blocks as a function of the number of segments, N_{bl}, per block. The straight lines indicate fits of the form $R_e^2 = b^2N_{bl} - c\sqrt{N_{bl}}$. (b) Mean square distance from the junction point, $R_e^2(s)$, as a function of the curvilinear distance, s.

VII. Conclusions and Outlook

Extensive Monte Carlo (MC) simulations of large AB-block-copolymer micelles in a B-homopolymer solvent have been quantitatively compared to self-consistent field (SCF) calculations utilizing the Gaussian chain model. By means of semi-grand-canonical identity switches in junction with multicanonical reweighting we investigated chains with up to $N = 128$ segments in the framework of the bond fluctuation model. The long chain length has proven crucial to make quantitative contact with the SCF predictions. A variety of properties including the aggregation number and its fluctuations, radial profiles to molecular conformations has been considered.

In the limit of very large chain lengths the MC data are compatible with the detailed predictions of the SCF calculations. Our comparisons reveal in several instances a rather slow convergence of the simulation "data" (which represent the exact statistical mechanics, including all fluctuation effects) to the theoretical predictions of the self-consistent field theory, with increasing chain length. This finding should be relevant for the use of this theory (as well as its simplified strong-stretching versions and related scaling arguments) to interpret experiments, too. Partially, the discrepancies for short chain length can be traced back to the small number of segments of the solvophobic block and the deviations from the Gaussian chain statistics due to excluded volume and local chain architecture on short length scales. Other deviations (in particular, the broadening of radial profiles) can be rationalized by fluctuations of the micelle shape which are ignored in the SCF calculations.

The comparison between MC data and SCF predictions shows that the deviations often decrease in relative importance like $1/\sqrt{N}$. The SCF calculation have also been extended to study the

dependence of the aggregation number and the critical micelle concentration on the incompatibility, χN. For the incompatibility considered in the simulation, $\chi N \approx 100$ the homopolymer solvent penetrates the corona. As χN increases, however, homopolymers are gradually expelled from the corona (dry brush, autophobicity) and, then, the additional free energy cost of the corona−melt interface tends to increase the micelle size.

This study of bulk micelles is a good starting point for investigating more complex situations like the adsorption of micelles on surfaces or interfaces and the structure of mixed micelles.

Acknowledgment. It is a great pleasure to thank C. Pastorino, T. Kreer, and J. P. Wittmer for stimulating discussions. Ample computing times was provided by the NIC, Jülich, Germany. A.C. gratefully acknowledges a fellowship from the Max-Planck Institut for Polymer Research, Mainz and additional financial support by the ESF Stipomat program. M.M. thanks the Volkswagen Foundation for support.

References and Notes

(1) Hamley, I. W. *The physics of block copolymers*; Oxford Science Publication: Oxford, U.K., 1998.
(2) Alexandridis, P.; Lindmann, B. *Amphiphilic block copolymers: self-assembly and applications*; Elsevier, Amsterdam, 2000.
(3) Riess, G. *Prog. Polym. Sci.* **2003**, *28*, 1107−1170.
(4) Leibler, L. *Makromol. Chem.−Macromol. Symp.* **1988**, *16*, 1−17.
(5) Shull, K. R.; Winey, K. I.; Thomas, E. L.; Kramer, E. J. *Macromolecules* **1991**, *24*, 2748−2751.
(6) Shull, K. R.; Kramer, E. J.; Hadziioannou, G.; Tang, W. *Macromolecules* **1990**, *23*, 4780−4787.
(7) Kataoka, K.; Kwon, G. S.; Yokoyama, M.; Okano, T.; Sakurai, Y. *J. Controlled Release* **1993**, *24*, 119−132.
(8) Kwon, G. S.; Kataoka, K. *Adv. Drug Delivery Rev.* **1995**, *16*, 295−309.
(9) Klingelhofer, S.; Heitz, W.; Greiner, A.; Oestreich, S.; Forster, S.; Antonietti, M. *J. Am. Chem. Soc.* **1997**, *119*, 10116−10120.
(10) Gelbart, W. M.; Benshaul, A. *J. Phys. Chem.* **1996**, *100*, 13169−13189.
(11) Leibler, L.; Orland, H.; Wheeler, J. C. *J. Chem. Phys.* **1983**, *79*, 3550−3557.
(12) Whitmore, M. D.; Noolandi, J. *Macromolecules* **1985**, *18*, 657−665.
(13) Birshtein, T. M.; Zhulina, E. B. *Polymer* **1990**, *31*, 1312.
(14) Izzo, D.; Marques, C. M. *Macromolecules* **1993**, *26*, 7189−7194.
(15) Sens, P.; Marques, C. M.; Joanny, J.-F. *Macromolecules* **1996**, *29*, 4880−4890.
(16) Izzo, D.; Marques, C. M. *Macromolecules* **1997**, *30*, 6544−6549.
(17) Zhulina, E. B.; Adam, M.; LaRue, I.; Sheiko, S. S.; Rubinstein, M. *Macromolecules* **2005**, *38*, 5330−5351.
(18) Semenov, A. N. *Macromolecules* **1993**, *26*, 2273−2281.
(19) Leibler, L.; Ajdari, A.; Mourran, A.; Coulon, G.; Chatenay, D. In *OUMS Conference on Ordering in Macromolecular Systems, Osaka*; Springer-Verlag: Berlin, 1994.
(20) Smit, B.; Hilbers, P. A. J.; Esselink, K.; Rupert, L. A. M.; Vanos, N. M.; Schlijper, A. G. *J. Phys. Chem.* **1991**, *95*, 6361−6368.
(21) Larson, R. G. *J. Chem. Phys.* **1992**, *96*, 7904−7918.
(22) Smit, B.; Esselink, K.; Hilbers, P.; van Os, N.; Rupert, L.; Szleifer, I. *Langmuir* **1993**, *9*, 9.
(23) Linse, P. *Macromolecules* **1993**, *26*, 4437−4449.
(24) Shelley, J. C.; Sprik, M.; Klein, M. L. *Langmuir* **1993**, *9*, 916−926.
(25) Wang, Y. M.; Mattice, W. L.; Napper, D. H. *Langmuir* **1993**, *9*, 66−70.
(26) Rector, D. R.; van Swol, F.; Henderson, J. R. *Mol. Phys.* **1994**, *82*, 1009−1031.
(27) Bernardes, A. T.; Henriques, V. B.; Bisch, P. M. *J. Chem. Phys.* **1994**, *101*, 645−650.
(28) Jan, N.; Stauffer, D. *J. Phys. I (Fr.)* **1994**, *4*, 345−350.
(29) Wijmans, C. M.; Linse, P. *Langmuir* **1995**, *11*, 3748−3756.
(30) Larson, R. *J. Phys. (Fr.) II* **1996**, *6*, 1441.
(31) Desplat, J. C.; Care, C. M. *Mol. Phys.* **1996**, *87*, 441−453.
(32) Mackie, A. D.; Tavitian, B.; Boutin, A.; Fuchs, A. *Mol. Simul.* **1997**, *19*, 1−16.
(33) Viduna, D.; Milchev, A.; Binder, K. *Macromol. Theory Simul.* **1998**, *7*, 649−658.
(34) Floriano, M. A.; Caponetti, E.; Panagiotopoulos, A. Z. *Langmuir* **1999**, *15*, 3143−3151.
(35) Milchev, A.; Binder, K. *Langmuir* **1999**, *15*, 3232−3241.
(36) Milchev, A.; Bhattacharya, A.; Binder, K. *Macromolecules* **2001**, *34*, 1881−1893.
(37) Farago, O. *J. Chem. Phys.* **2003**, *119*, 596.
(38) Brannigan, G.; Brown, F. *J. Chem. Phys.* **2004**, *120*, 1059.
(39) Cooke, I.; Kremer, K.; Deserno, M. *Phys. Rev. E* **2005**, *72*, 011506.
(40) Brannigan, G.; Brown, F. *J. Chem. Phys.* **2005**, *122*, 074905.
(41) Cooke, I. R.; Deserno, M. *J. Chem. Phys.* **2005**, *123*, 224710.
(42) Brannigan, G.; Lin, L. C. L.; Brown, F. L. H. *Eur. Biophys. J.* **2006**, *35*, 104−124.
(43) Chang, R. W.; Yethiraj, A. *J. Chem. Phys.* **2001**, *114*, 7688−7699.
(44) Müller, M.; Binder, K. *Macromolecules* **1995**, *28*, 1825−1834.
(45) Müller, M.; Werner, A. *J. Chem. Phys.* **1997**, *107*, 10764−10776.
(46) Werner, A.; Schmid, F.; Müller, M.; Binder, K. *Phys. Rev. E* **1999**, *59*, 728−738.
(47) Carmesin, I.; Kremer, K. *Macromolecules* **1988**, *21*, 2819.
(48) Deutsch, H. P.; Binder, K. *J. Chem. Phys.* **1991**, *94*, 2294−2304.
(49) Müller, M. *Macromol. Theory Simul.* **1999**, *8*, 343−374.
(50) Müller, M. *Macromolecules* **1995**, *28*, 6556−6564.
(51) Sariban, A.; Binder, K. *J. Chem. Phys.* **1987**, *86*, 5859−5873.
(52) Deutsch, H. P.; Binder, K. *Macromolecules* **1992**, *25*, 6214−6230.
(53) Müller, M.; Binder, K. *Macromolecules* **1998**, *31*, 8323−8346.
(54) Müller, M.; Schick, M. *J. Chem. Phys.* **1996**, *105*, 8885−8901.
(55) Müller, M.; Schick, M. *J. Chem. Phys.* **1996**, *105*, 8282−8292.
(56) Berg, B. A.; Neuhaus, T. *Phys. Rev. Lett.* **1992**, *68*, 9.
(57) Berg, B. A.; Hansmann, U.; Neuhaus, T. *Phys. Rev. B* **1993**, *47*, 497.
(58) Berg, B.; Hansmann, U.; Neuhaus, T. *Z. Phys* **1993**, *B 90*, 229.
(59) Müller, M.; Binder, K.; Oed, W. *J. Chem. Soc., Faraday Transactions* **1995**, *91*, 2369−2379.
(60) Virnau, P.; Müller, M. *J. Chem. Phys.* **2004**, *120*, 10925−10930.
(61) Helfand, E.; Tagami, Y. *J. Polym. Sci., Part B: Polym. Lett.* **1971**, *9*, 741.
(62) Scheutjens, J. M. H. M.; Fleer, G. J. *J. Phys. Chem.* **1979**, *83*, 1619−1635.
(63) Hong, K. M.; Noolandi, J. *Macromolecules* **1981**, *14*, 727−736.
(64) Noolandi, J.; Hong, K. M. *Macromolecules* **1983**, *16*, 1443−1448.
(65) Whitmore, M. D.; Noolandi, J. *Macromolecules* **1988**, *21*, 1482−1496.
(66) Matsen, M. W.; Schick, M. *Phys. Rev. Lett.* **1994**, *72*, 2660−2663.
(67) Matsen, M. W. *Macromolecules* **1995**, *28*, 5765−5773.
(68) Shi, A. C.; Noolandi, J.; Desai, R. C. *Macromolecules* **1996**, *29*, 6487−6504.
(69) Laradji, M.; Shi, A. C.; Noolandi, J.; Desai, R. C. *Macromolecules* **1997**, *30*, 3242−3255.
(70) Fredrickson, G. H.; Ganesan, V.; Drolet, F. *Macromolecules* **2002**, *35*, 16−39.
(71) Matsen, M. W. *J. Chem. Phys.* **1999**, *110*, 4658−4667.
(72) Müller, M.; Gompper, G. *Phys. Rev. E* **2002**, *66*, 041805.
(73) Müller, M.; MacDowell, L. G.; Virnau, P.; Binder, K. *J. Chem. Phys.* **2002**, *117*, 5480−5496.
(74) Duque, D. *J. Chem. Phys.* **2003**, *119*, 5701−5704.
(75) Müller, M.; Schick, M. *J. Chem. Phys.* **1996**, *105*, 8282−8292.
(76) Müller, M. *Macromolecules* **1998**, *31*, 9044−9057.
(77) Semenov, A. N. *Zh. Eksp. Teor. Fiz.* **1985**, *88*, 1242−1256.
(78) Paul, W.; Binder, K.; Heermann, D. W.; Kremer, K. *J. Phys. II (Fr.)* **1991**, *1*, 37−60.
(79) Semenov, A. N. *J. Phys. II (Fr.)* **1996**, *6*, 1759−1780.
(80) Likhtman, A. E.; Semenov, A. N. *Europhys. Lett.* **2000**, *51*, 307.

MA061493G